PASJ: Publ. Astron. Soc. Japan **59**, 55–60, 2007 February 25

ASTE Observations of Nearby Galaxies: A Tight Correlation between CO ($J = 3$–2) Emission and Hα

Shinya KOMUGI,[1,3] Kotaro KOHNO,[1] Tomoka TOSAKI,[2] Hiroyuki NAKANISHI,[2]
Sachiko ONODERA,[1] Fumi EGUSA,[1] and Yoshiaki SOFUE[1]
[1] *Institute of Astronomy, The University of Tokyo, 2–21–1 Osawa, Mitaka-shi, Tokyo 181–8588*
[2] *Nobeyama Radio Observatory, Minamimaki, Minamisaku, Nagano 384-1305*
[3] *National Astronomical Observatory of Japan, 2–21–1 Osawa, Mitaka-shi, Tokyo 181–8588*
skomugi@ioa.s.u-tokyo.ac.jp

(Received 2006 July 19; accepted 2006 October 16)

Abstract

Star formation rates (*SFR*s) obtained via extinction-corrected Hα are compared to dense gas, as traced by ^{12}CO ($J = 3$–2) emission at the centers of nearby galaxies, observed with the ASTE telescope. It is found that, although many of the observed positions are dusty, and therefore heavily absorbed at Hα, the *SFR* shows a striking correlation with dense gas in the form of the Schmidt law with an index of 1.0. The correlation is also compared between gas traced by ^{12}CO ($J = 1$–0) and the application of an Hα extinction correction. We find that dense gas produces a far-better correlation with *SFR* in view of the surface density values.

Key words: galaxies: ISM — galaxies: spiral — ISM: molecules — stars: formation

1. Introduction

The present knowledge of star formation on galactic scales in relation with its precursor gas is generally expressed by the Schmidt law (Schmidt 1959),

$$SFR \propto \rho^N, \tag{1}$$

where SFR is the star-formation rate, ρ the gas density, and N the Schmidt law index, expressing the efficiency of star formation from gas. Often written also in terms of surface averaged quantities, equation (1) relates two physical values, SFR and ρ, which are generally spatially decoupled when observed locally, and connected in a spatially averaged sense. The connection between the two values also has a time-averaged nature, namely the formation timescale of massive stars. Therefore, in order to obtain valid physical suggestions from the Schmidt law, we must derive these two values based on measurements that express conditions that are spatially and temporally connected as much as observations allow.

Previous observations of molecular gas have been conducted mainly in the ^{12}CO ($J = 1$–0) line (e.g., Komugi et al. 2005), tracing cold gas that constitutes the bulk of galactic molecular clouds. However, Kohno et al. (1999) have shown that a tracer of denser gas, HCN, shows a better spatial correlation with the star-forming regions. Observations of *dense* gas tracers, such as HCN (Gao & Solomon 2004), and higher transition CO lines, like ^{12}CO ($J = 2$–1) (Braine et al. 1993; Böker et al. 2003) and ^{12}CO ($J = 3$–2) (Mauersberger et al. 1999; Yao et al. 2003; Narayanan et al. 2005), are becoming accessible, and it is of interest how these tracers of dense gas show up in terms of the Schmidt law.

The calibration of *SFR* becomes an issue under these circumstances, where virtually all observational inquiry of the Schmidt law using dense gas has resorted to FIR as the *SFR* calibrator. This in part is due to the fact that FIR data from the IRAS satellite is abundant, and that many of the sample galaxies observed in dense gas tracers (HCN and higher CO transitions) were selected according to the FIR luminosity. However, we must bear in mind that the *SFR* must be calibrated using *massive* stars. The *SFR* derived from the FIR luminosity can only trace star formation over $\sim 10^8$ years, because of its contamination from extended dust heated by the interstellar radiation field (Kennicutt 1998), which can amount to a significant fraction of the FIR luminosity (e.g., Hirashita et al. 2003).

This results in an overestimation of the *SFR*, and also becomes a bottleneck in improving the temporal connection of gas and star formation. Another practical shortage is that the angular resolution of IRAS data is commonly several arcminutes, too large to infer physics from the correlation between dense gas tracer data, which are typically tens of arcseconds in angular resolution. The most reliable massive *SFR* tracer to date is the Hα luminosity, tracing star formation over several 10^6 years, whose correlation with dense gas has surprisingly not been checked. The main reason is that Hα is weak in dusty galaxies, such as those observed in dense gas tracers, due to extinction within the galaxies. It is therefore important not only to acquire the Hα luminosity of these galaxies, but to accurately estimate the amount of extinction.

The main objective and result of this paper is to examine the correlation between ^{12}CO ($J = 3$–2) tracing warm dense gas (typically ~ 30 K), and *extinction-corrected* Hα luminosity, accurately tracing the *SFR* in surface averaged densities.

2. Observation

Observations of ^{12}CO ($J = 3$–2) at 345 GHz were conducted using the Atacama Submillimeter Telescope Experiment (ASTE) (Ezawa et al. 2004; Kohno 2005), a 10 m single dish located in the Atacama desert at an altitude of 4800 m in Pampa La Bola, Chile. Observations were made remotely

Table 1. Observed galaxies.*

Galaxy	RA	DEC	Morphology	D	i	$I_{\rm CO}^{3-2}$	$\log\Sigma_{SFR}$	$\log\Sigma_{SFR}^{\rm corr}$
	1950	1950		Mpc	deg	K km s^{-1}	$M_\odot$ pc^{-2} yr^{-1}	
(1)	(2)	(3)	(4)	(5)	(6)	(7)	(8)	(9)
NGC 157	00 32 14.45	−08 40 18.8	SABbc	35	49	6.9±0.5	−7.58	
NGC 520	01 21 59.79†	+03 31 55.9†	Pec	45.5	66	no detection		
NGC 925	02 24 16.89	+33 21 18.9	SABd	14.3	53	1.1±0.5	−7.70	
NGC 1022	02 36 03.99	−06 53 34.1	SBa	30.1	34	45 ±1.0		
NGC 1068	02 40 07.05	−00 13 31.6	SAb	22.7	40	157 ±4.5		
	02 40 06.50†	−00 13 32.0†				129 ±3.8	−5.42	−4.92
NGC 1084	02 43 32.11	−07 47 17.4	SAc	28.1	59	19 ±1.7		
	02 43 31.80†	−07 47 06.0†				13.4±1.0	−7.51	
NGC 1087	02 43 51.88	−00 42 28.4	SABc	36.9	49	10.3±0.5		
	02 43 51.60†	−00 42 19.0†				8.3±0.2	−7.17	
NGC 7479	23 02 26.39	+12 03 10.3	SBc	52.1	38	21.3±0.9		
	23 02 26.80†	+12 03 06.0†				15.9±0.8	−7.77	−6.74
NGC 7625	23 17 60.00	+16 57 05.6	SAa pec	37.3	22	24.3±0.8		
	23 18 00.60†	+16 57 15.0†				11.3±0.5		

* (1) Galaxy name. (2)(3) Coordinates from NED. Many were observed also at optically defined coordinates from Dressel and Condon (1976), used in the ^{12}CO (J = 1–0) survey by S. Komugi et al. (in preparation), marked †. For NGC 157 and NGC 925, coordinates from both NED and Dressel and Condon (1976) match. (4)(5)(6) Morphology, distance, and inclination in degrees, as listed in Young et al. (1995). (7) Observed integrated intensity of ^{12}CO (J = 3–2), converted to main beam temperature units. (8)(9) *SFR* and extinction corrected *SFR*, respectively, as explained in text.

from an ASTE operation room of the National Astronomical Observatory of Japan (NAOJ) at Mitaka, Japan, using a network observation system, N-COSMOS3, developed by NAOJ (Kamazaki et al. 2005).

The sample was selected to be able to compare the dense gas quantity and its relation with star formation, in both normal and starbursting galaxies. The galaxies were selected so that most of them have readily accessible and extinction correctable Hα data. Another limitation for the samples was that their velocity width had to be under 350 km s^{-1}, chosen so that the emission would fit within a bandwidth of 445 km s^{-1} of the backend, allowing for baseline subtraction. Table 1 lists the observed samples. The galaxies were observed only at their central position, and the resolution width of ASTE (22″ in FWHM) corresponds to a linear size of $\sim$ 3 kpc for a typical sample distance of 30 Mpc.

The observations were conducted in 2005 August, under fair weather conditions, using a double-sideband cooled SIS mixer. Calibration was done using the standard chopper wheel method. The backend was a 1024 channel digital spectrometer with a 512 MHz bandwidth and a frequency resolution of 0.5 MHz, corresponding to a velocity resolution of 0.43 km s^{-1}. The resulting velocity bandwidth was 445 km s^{-1}. Typical system temperatures at 345 GHz ranged from 180 K to 300 K. The pointing was checked every several hours using Uranus or Mars, and was found to be accurate to $\sim 1''$.

The obtained data were reduced with NEWSTAR, an AIPS-based software, used commonly at Nobeyama Radio Observatory (NRO). After flagging bad spectra, first to second-order baselines were subtracted, then smoothed to a velocity resolution of typically 15 to 20 km s^{-1}. $T_{\rm A}^*$ was then converted to $T_{\rm mb}$ via $T_{\rm mb} = T_{\rm A}^*/0.6$, where 0.6 is the main beam efficiency of the ASTE telescope. The resultant integrated intensities of the galaxies are listed in table 1.

3. Results

The integrated intensity, $I_{\rm CO}(J=3\text{–}2) = \int T_{\rm mb} dv$, can be converted to surface gas density using the conversion factor $X_{\rm CO}$, such that $\Sigma \propto X_{\rm CO} I_{\rm CO}$, assuming that ^{12}CO (J = 3–2) uniquely traces dense gas.

However, the gas temperature can contribute to ^{12}CO (J = 3–2) emission, and will introduce complications. In order to circumvent this difficulty, we use $I_{\rm CO}$ (J = 3–2) hereafter, regardless of what it implies physically. The errors for the values listed in table 1 were calculated using

$$\delta I_{\rm CO} = \sigma \sqrt{\Delta V_{\rm CO} \delta V} \quad ({\rm K\ km\ s^{-1}}), \tag{2}$$

where σ is the r.m.s. noise in $T_{\rm mb}$, $\Delta V_{\rm CO}$ the full line width, and δV is the velocity resolution (15 or 20 km s^{-1}). The obtained spectra are presented in figure 1.

All galaxies were detected, except for NGC 520; we attribute this to NGC 520's line width of 500 km s^{-1}, from Solomon et al. (1992).

3.1. SFR

The *SFR* was derived for the sample galaxies where possible, using narrow-band Hα imaging data from Young et al. (1996). The flux within the ASTE beam was calculated using task "apphot" on the FITS images using IRAF software. The *SFR* surface density, Σ_{SFR}, was then calculated using the formulation by Kennicutt (1998), and corrected for inclination by a factor of $\cos i$.

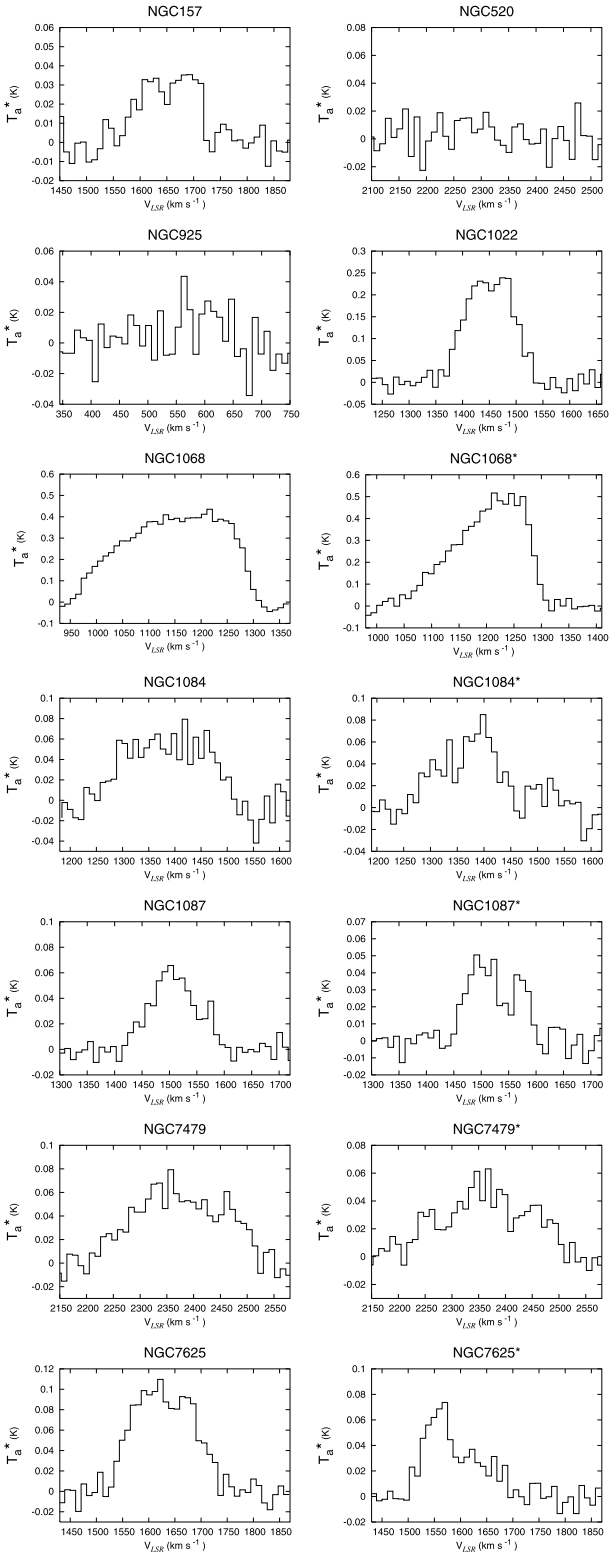

Fig. 1. ^{12}CO (J = 3–2) spectra of the galaxy centers observed at ASTE. Spectra with an asterisk are those observed at positions indicated by a dagger in table 1.

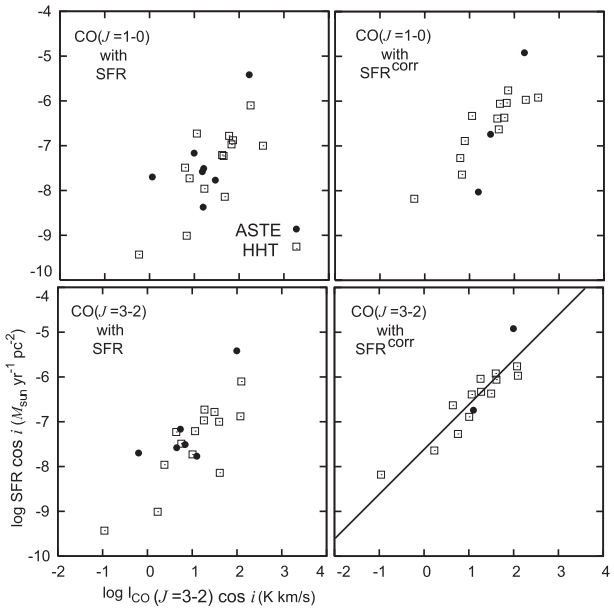

Fig. 2. Obtained Schmidt law for the sample galaxies, using combinations of gas [^{12}CO (J = 1–0) and ^{12}CO (J = 3–2)], and *SFR* with and without an internal extinction correction. The lower right hand panel is best correlated, with N = 1.0 shown as the best fit line.

$$\Sigma_{SFR}(M_\odot \mathrm{pc}^{-2}\mathrm{yr}^{-1}) = 7.9\times10^{-42}\frac{L(\mathrm{H}\alpha)}{S}\cos i\ (\mathrm{erg\ s}^{-1}\mathrm{pc}^{-2}), \quad (3)$$

where S is the projected area of the observing beam. The *SFR* derived in this way was then corrected for internal extinction into $\Sigma_{SFR}^{\mathrm{corr}}$ when possible, by dust using $E(B-V)$ magnitudes derived from the Hα/Hβ ratio given in Ho et al. (1997). Combined with equation (3), we obtained the extinction corrected SFR $\Sigma_{SFR}^{\mathrm{corr}}$.

In order to compensate for the lack of data, we compiled ^{12}CO (J = 3–2) from other sources. table 2 lists these sources, along with the *SFR* derived as above, where possible.

3.2. *Schmidt Law*

Figure 2 shows the obtained Schmidt law between extinction-corrected Hα and ^{12}CO (J = 3–2). For a comparison, we also show the relation between ^{12}CO (J = 1–0) and Hα. ^{12}CO (J = 1–0) data were taken from similar resolution (16″ or 22″) surveys by S. Komugi et al. (in preparation), Braine et al. (1993), and Nishiyama and Nakai (2001). Apparently, a combination of extinction-corrected *SFR* and dense gas gives a better correlation. Table 3 gives the Schmidt law index, N, and the correlation coefficient. In all cases, the index, N, of the Schmidt law is found to be effectively 1, consistent with previous studies that used the total luminosity when comparing the two values representing gas and *SFR* (Gao & Solomon 2004; Yao et al. 2003; Böker et al. 2003), even though we used surface densities, which are more indicative of the intrinsic properties of the samples.

3.3. *Inclination Correction*

An effect that we must consider when using surface averaged values is the inclination of the target galaxy, where the

Table 2. Sample galaxies.*

Galaxy	Reference	$I_{\rm CO}^{3-2}$	$\log \Sigma_{SFR}$	$\log \Sigma_{SFR}^{\rm corr}$
		K km s^{-1}	$M_\odot$ pc^{-2} yr^{-1}	
(1)	(2)	(3)	(4)	(5)
NGC 891	1	24 ±2	−9.01	−7.64
NGC 2146	1	193	−6.88	−5.76
NGC 2276	2	12.2±0.2	−7.21	−6.39
NGC 2903	1	63 ±2	−6.78	−6.37
NGC 3079	2	183 ±3.2	−8.14	−6.06
NGC 3351	1	28	−6.73	−6.33
NGC 3627	1	8.8±1	−7.23	−6.63
NGC 4088	1	26 ±1	−7.73	−6.89
NGC 4102	1	31	−6.97	−6.04
NGC 5907	1	6 ±0.7	−9.43	−8.18
NGC 6946	1	46 ±2	−7.00	−5.92
NGC 7331	1	17.5±1.2	−7.49	−7.27
NGC 7541	1	7 ±1	−7.96	—

* (1) Galaxy name. (2) References. 1 refers to Mauersberger et al. (1999), 2 refers to Narayanan et al. (2005). Both were observed at the HHT, with an angular resolution of 22″, same as ASTE. (3) Integrated intensity of ^{12}CO (J = 3–2) line, in main beam temperature units. (4)(5) *SFR* and extinction corrected *SFR*, respectively.

Table 3. Least squares fit.*

Gas tracer	Ext. Corr.	N	r^2
(1)	(2)	(3)	(4)
^{12}CO (J = 3–2)	Yes	0.93±0.12	0.91
		0.86±0.19	0.78
^{12}CO (J = 1–0)	Yes	1.05±0.19	0.83
		1.00±0.30	0.41
^{12}CO (J = 3–2)	No	0.92±0.17	0.79
		0.60±0.21	0.57
^{12}CO (J = 1–0)	No	0.93±0.22	0.70
		0.48±0.25	0.41

* (1) Tracer used for dense gas. (2) "No" for no Hα extinction correction, "Yes" for correction applied as explained in text. (3)(4) Schmidt law index N and correlation coefficient, from a least squares fitting. For all gas tracers, the lower row is for no inclination correction.

surface density is derived by multiplying the luminosity by $\cos i$. However, inclination is generally defined from its global morphology, and hence is not always indicative of the disk in its central kpc, as in this case. The central region may be thick or clumpy, so that corrections for inclination are not necessary in the first place. To see if a factor of $\cos i$ is justified, we plot the inclination-corrected gas densities and *SFR* vs. $\cos i$ on the left-hand side of figure 3. Apparently, the values decrease with increasing inclination (i.e., as they become edge-on), a trend that should not be seen if the correction is correct, because the inclination of galaxies is a meaningless parameter regarding its intrinsic properties, and the average face-on surface density should be independent of the inclination. The decreasing trend is roughly the same for ^{12}CO (J = 1–0), ^{12}CO (J = 3–2), and

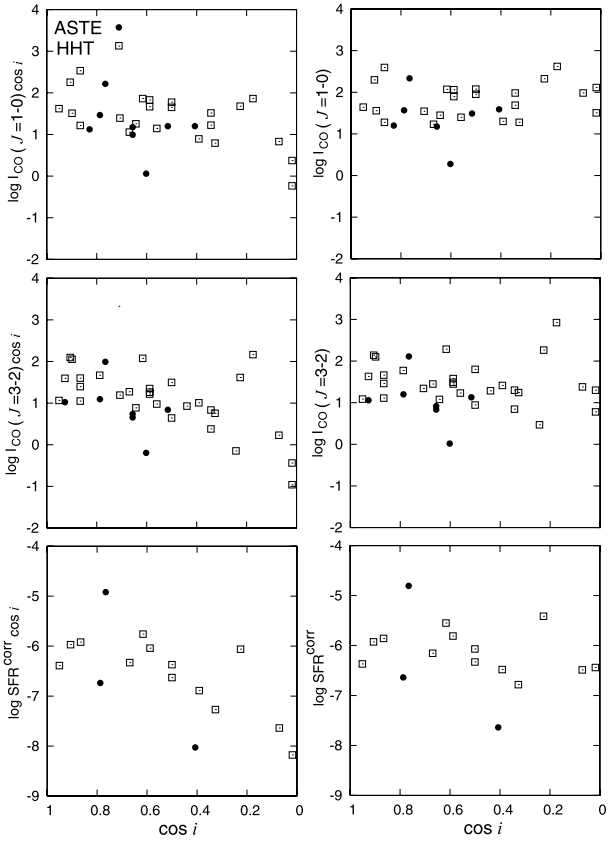

Fig. 3. Inclination versus surface gas density and *SFR* density, corrected for (left) and uncorrected for inclination (right). Notice that the figures on the left show a decreasing density with the inclination, whereas the figures on the right show no trend.

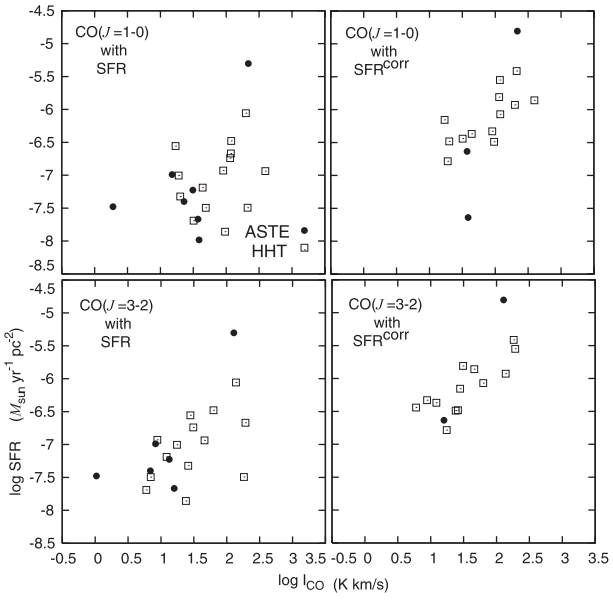

Fig. 4. Same as figure 2, but uncorrected for inclination. ^{12}CO (J = 3–2) with corrected *SFR* (correlation coefficient 0.78) still shows a better correlation compared to ^{12}CO (J = 1–0) (correlation coefficient 0.41).

SFR, which suggests that this trend is not due to the opacity of the emission lines, but more of a geometric quality, i.e., that the structure inside the 22″ beam is more clumpy than disky. The resulting Schmidt law will be biased towards $N = 1$, because the gas and *SFR* densities decrease equally along a slope of 1. The right hand side of figure 3, is the same for values uncorrected for inclination. We do not see any trend with inclination, which is physically more plausible.

From these views, we conclude that a correction for inclination of $\cos i$ is not completely justified; figure 4 show the Schmidt law for all values uncorrected for inclination. The variance of the residuals for a best fit is given in table 3; in this case, we can also see that the use of ^{12}CO (J = 3–2) and extinction-corrected Hα greatly improves the fit.

4. Discussion

We have shown for the first time that ^{12}CO (J = 3–2) has a striking correlation with Hα-derived *SFR*. Assuming that ^{12}CO (J = 3–2) indeed traces dense gas, this implies that Hα may be a valid *SFR* tracer, even in dense and dusty regions. Dense gas ^{12}CO (J = 3–2) also correlates better with recent star formation compared to ^{12}CO (J = 1–0).

Interpreting this result in a qualitative manner is easy. Assuming that star formation occurs where gas density exceeds a certain value, we can expect that ^{12}CO (J = 3–2) is more spatially and temporally connected to star formation compared to ^{12}CO (J = 1–0). By using Hα as a *SFR* tracer, the spatial connection (resolution) and the temporal connection (traces SF over 10^6 years) are even more improved. This improvement should show up in terms of the Schmidt law.

Using Hα, we have circumvented the need to use global gas and *SFR* in expressing the Schmidt law, which is known to introduce a size effect. Larger galaxies tend to be more luminous at any wavelength: therefore producing a correlation between gas and *SFR* without any other physical reasons (see Stark et al. 1986). The resolution of Hα imaging allowed us to meaningfully derive the surface density values, whereas using the IRAS data may force us to compare spatially decoupled gas and *SFR* within the large beam.

The Schmidt law index, N, however, should be treated with care. The correction for extinction can be applied only to detectable emission, and not the intrinsic total Hα emission. This is not unique to recombination lines, but to all star-formation tracers where extinction plays a role. In that light, The observed Schmidt law index is always an underestimate, where in our case the effect may be strong because our study focuses on the central regions of dusty galaxies. This is in concord with the literature, where the widely accepted value of 1.4 (e.g., Kennicutt 1998) is considerably higher than our derived value of ~ 1.0.

The authors thank Judy S. Young, for kindly providing us with narrow-band Hα images. S.K., S.O., and F.E. were financially supported by a Research Fellowship from the Japan Society for the Promotion of Science for Young Scientists. This study was financially supported by the MEXT Grant-in-Aid for Scientific Research on Priority Areas No. 15071202. Observations with ASTE were in part carried out remotely from Japan by using NTT's GEMnet2 and its partner R&E (Research and Education) networks, which are based on AccessNova collaboration of University of Chile, NTT Laboratories, and National Astronomical Observatory of Japan. This paper has made use of the NASA/IPAC Extragalactic Database (NED), which is operated by the Jet Propulsion Laboratory, Caltech, under contract with the National Aeronautics and Space Administration.

References

Böker, T., Lisenfeld, U., & Schinnerer, E. 2003, A&A, 406, 87
Braine, J., Combes, F., Casoli, F., Dupraz, C., Gerin, M., Klein, U., Wielebinski, R., & Brouillet, N. 1993, A&AS, 97, 887
Dressel, L. L., & Condon, J. J. 1976, ApJS, 31, 187
Ezawa, H., Kawabe, R., Kohno, K., & Yamamoto, S. 2004, Proc. SPIE, 5489, 763
Gao, Y., & Solomon, P. M. 2004, ApJ, 606, 271
Hirashita, H., Buat, V., & Inoue, A. K. 2003, A&A, 410, 83
Ho, L. C., Filippenko, A. V., & Sargent, W. L. W. 1997, ApJS, 112, 315
Kamazaki, T., et al. 2005, ASP Conf. Ser., 347, 533
Kennicutt, R. C., Jr. 1998, ARA&A, 36, 189
Kohno, K. 2005, ASP Conf. Ser., 344, 242
Kohno, K., Kawabe, R., & Vila-Vilaró, B. 1999, ApJ, 511, 157
Komugi, S., Sofue, Y., Nakanishi, H., Onodera, S., & Egusa, F. 2005, PASJ, 57, 733
Mauersberger, R., Henkel, C., Walsh, W., & Schulz, A. 1999, A&A, 341, 256
Narayanan, D., Groppi, C. E., Kulesa, C. A., & Walker, C. K. 2005, ApJ, 630, 269

Nishiyama, K., & Nakai, N. 2001, PASJ, 53, 713
Schmidt, M. 1959, ApJ, 129, 243
Solomon, P. M., Downes, D., & Radford, S. J. E. 1992, ApJ, 387, L55
Stark, A. A., Knapp, G. R., Bally, J., Wilson, R. W., Penzias, A. A., & Rowe, H. E. 1986, ApJ, 310, 660
Yao, L., Seaquist, E. R., Kuno, N., & Dunne, L. 2003, ApJ, 588, 771
Young, J. S., et al. 1995, ApJS, 98, 219
Young, J. S., Allen, L., Kenney, J. D. P., Lesser, A., & Rownd, B. 1996, AJ, 112, 1903